Research Article

Physics-Informed Neural Networks for Exterior Potential Flow Around a Circular Cylinder Without Far-Field Boundary Conditions

Y. Jangid[1], **Der-Liang Young**[2,3]

1. Department of Civil Engineering, MBM University, Jodhpur, India; 2. Department of Civil Engineering, National Taiwan University, Taiwan, Province of China; 3. Core Tech System Co. Ltd, Moldex3D, Taiwan

Physics-informed neural networks (PINNs) have emerged as a promising framework for solving partial differential equations by embedding physical laws directly into the learning process. While PINNs have shown strong performance for bounded-domain problems, their application to exterior flow problems typically relies on artificial far-field boundary conditions to truncate the computational domain. In this work, we investigate the capability of PINNs to solve the exterior potential flow around a circular cylinder using only the solid boundary condition, without imposing any far-field constraints.

The governing Laplace equation for the stream function is enforced through the physics-informed loss, while the no-penetration condition on the cylinder surface is prescribed as the sole boundary condition. Numerical results demonstrate that the proposed PINN accurately recovers the stream function, velocity field, and pressure coefficient distribution throughout the exterior domain. Despite the absence of far-field boundary conditions, the learned solution exhibits physically consistent far-field behaviour within the sampled domain, strong agreement with analytical solutions, and low global and maximum errors.

These results indicate that, for classical potential flow problems, PINNs can infer physically consistent far-field behaviour directly from the governing equations and solid boundary information alone. The findings provide new insight into the behaviour of PINNs in unbounded domains and highlight their potential for solving exterior flow problems without reliance on artificial boundary truncation.

Corresponding authors: D.L. Young, dlyoung@ntu.edu.tw; Y. Jangid, Yashs99834@gmail.com

doi.org/10.32388/IN02KQ

1. Introduction

The simulation of fluid flow around solid bodies is a fundamental problem in fluid mechanics with broad applications in aerodynamics, hydrodynamics, and engineering design. Among classical benchmark problems, the two-dimensional incompressible and irrotational flow around a circular cylinder plays a central role due to its analytical tractability and well-understood physical characteristics. The problem serves as a standard test case for assessing numerical methods and data-driven approaches for solving partial differential equations in exterior domains.

Traditional numerical methods for solving exterior flow problems, such as finite difference, finite volume, and finite element methods, typically require the introduction of artificial far-field boundaries to truncate the unbounded physical domain. Appropriate boundary conditions must then be imposed at these fictitious boundaries to approximate the behaviour at infinity. While effective, this approach introduces additional modelling assumptions and may influence the accuracy and stability of the numerical solution, particularly when the far-field behaviour is not known a priori.

Physics-informed neural networks (PINNs) have recently attracted significant attention as an alternative framework for solving partial differential equations [1][2]. By embedding governing equations and boundary conditions directly into the loss function, PINNs enable the approximation of solution fields without the need for mesh generation or labelled training data. Since their introduction, PINNs have been successfully applied to a wide range of problems involving elliptic, parabolic, and hyperbolic equations [1][2][3][4].

Despite these advances, most existing PINN studies addressing exterior flow problems continue to rely on artificial far-field boundary conditions to ensure well-posedness and numerical stability. The extent to which PINNs can infer correct far-field behaviour solely from the governing equations and solid boundary information remains an open question. Understanding this capability is particularly important for unbounded-domain problems, where the introduction of fictitious boundaries may be undesirable or impractical.

In this work, we investigate the performance of physics-informed neural networks for the classical exterior potential flow around a circular cylinder, with a specific focus on eliminating far-field boundary conditions altogether. The stream function formulation is adopted, and the Laplace equation governing incompressible, irrotational flow is enforced throughout the domain. The only prescribed boundary condition is the no-penetration condition on the surface of the cylinder.

The objectives of this study are threefold:

1. To assess whether a PINN can recover the correct exterior flow solution using only the solid boundary condition.
2. To evaluate the accuracy of the resulting stream function, velocity field, and pressure coefficient distribution in the absence of far-field constraints.
3. To analyse the error structure and stability of the learned solution in an unbounded domain.

Through extensive numerical experiments and detailed error analysis, we demonstrate that the proposed PINN accurately reproduces the analytical solution with low global and maximum errors, despite the absence of explicit far-field boundary enforcement. The results provide new insight into the behaviour of PINNs for exterior problems and highlight their potential for modelling unbounded flows using minimal boundary information.

2. Governing Equations and Classical Solution

In this study, we consider the two-dimensional incompressible and irrotational flow of an inviscid fluid around a circular cylinder of radius a placed in a uniform free stream of velocity U. Under these assumptions, the flow can be described using potential flow theory, for which the velocity field is derived from a scalar potential or, equivalently, from a stream function formulation.

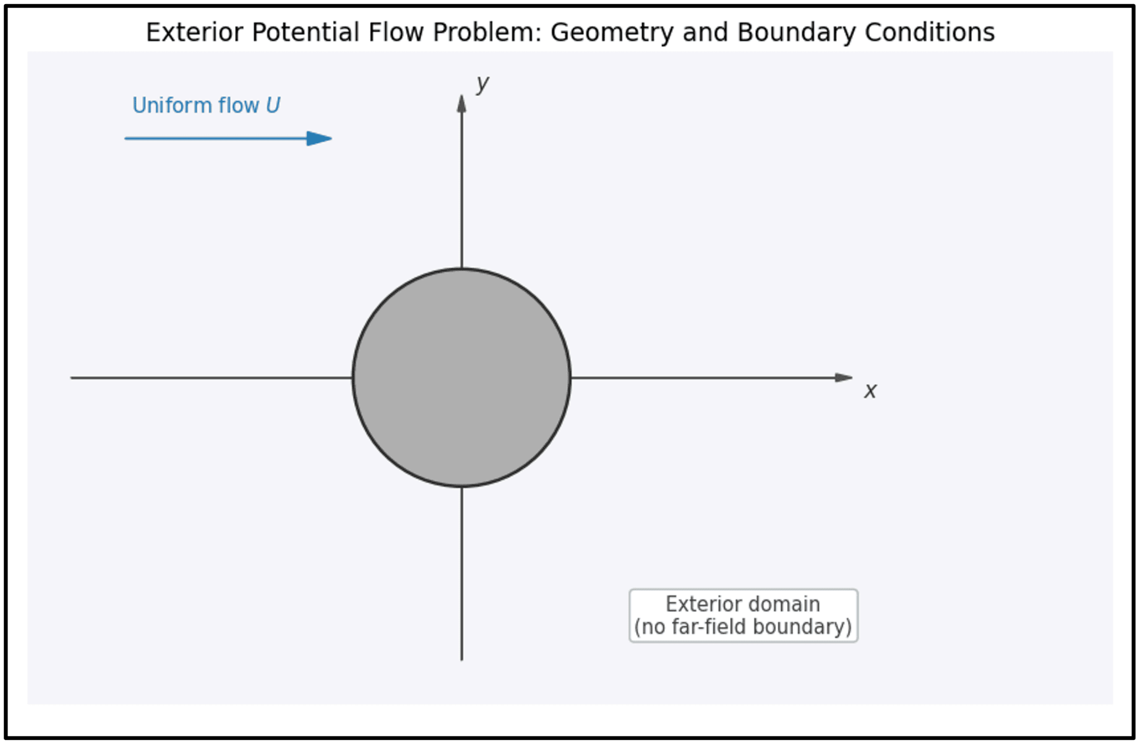

Figure 1. Schematic of the exterior potential flow problem around a circular cylinder of radius a in a uniform free stream of velocity U. The governing equation is enforced in the exterior domain, while the no-penetration condition $\psi = 0$ is prescribed on the cylinder surface. No far-field boundary condition is imposed.

2.1. Stream Function Formulation

For incompressible flow, the velocity field $u = (u, v)$ satisfies the $\nabla \cdot u = 0$.

In two dimensions, this condition is automatically satisfied by introducing a stream function $\psi(x, y)$ such that

$$u = \frac{\partial\psi}{\partial y}, v = -\frac{\partial\psi}{\partial x}.$$

For irrotational flow, the vorticity vanishes, leading to the condition

$$\nabla \times u = 0.$$

Substituting the stream function definition into the vorticity-free condition yields the governing equation

$$\nabla^2\psi = 0,$$

doi.org/10.32388/IN02KQ

which is the Laplace equation. Therefore, the stream function for incompressible, irrotational flow satisfies a second-order elliptic partial differential equation throughout the flow domain.

2.2. Boundary Conditions for Exterior Cylinder Flow

The physical domain of interest is the exterior region $\Omega = \mathbb{R}^2 \setminus \{r \leq a\}$, where $r = \sqrt{x^2 + y^2}$. On the surface of the cylinder, the no-penetration condition requires that the normal component of velocity vanish. In terms of the stream function, this condition implies that $\psi$is constant along the solid boundary. Without loss of generality, the stream function on the cylinder surface is set to zero:

$$\psi(r = a) = 0.$$

In classical formulations, an additional far-field condition is imposed to enforce uniform flow behaviour as $r \to \infty$, typically of the form

$$\psi \sim Uy\text{as } r \to \infty.$$

In the present work, however, no such far-field boundary condition is prescribed. The governing equation is enforced throughout the exterior domain, and the no-penetration condition on the cylinder surface is the only boundary condition applied. The ability of the physics-informed neural network to infer the correct asymptotic behaviour from this minimal information is a central focus of this study.

2.3. Velocity Potential Formulation

For incompressible and irrotational flow, the velocity field can also be expressed in terms of a scalar velocity potential $\phi(x, y)$. The velocity components are defined as

$$u = \frac{\partial \phi}{\partial x}, v = \frac{\partial \phi}{\partial y}.$$

Irrotationality of the flow implies that the velocity potential satisfies the Laplace equation,

$$\nabla^2 \phi = 0,$$

throughout the exterior domain Ω. As a result, both the stream function $\psi$and the velocity potential $\phi$are harmonic functions that describe the same physical flow field.

For the exterior potential flow around a circular cylinder of radius $a$in a uniform free stream of velocity U, the classical analytical expression for the velocity potential in polar coordinates $(r, \theta)$is given by

$$\phi(r, \theta) = U\left(r + \frac{a^2}{r}\right)\cos\theta.$$

This solution satisfies the Laplace equation in the exterior domain and represents uniform flow perturbed by the presence of the solid cylinder. The corresponding stream function, given in Section 2.2, is orthogonal to the velocity potential, and the two functions together form a harmonic conjugate pair.

The equipotential lines $\phi = \mathrm{constant}$are everywhere orthogonal to the streamlines $\psi = \mathrm{constant}$. This orthogonality property provides a useful physical interpretation of the flow field and serves as an additional qualitative validation of numerical solutions. In the present work, equipotential lines are used in conjunction with streamlines to assess the physical consistency of the PINN-predicted flow field.

2.4. Classical Analytical Solution

For reference and validation, the analytical solution for the potential flow around a circular cylinder in a uniform stream is briefly summarized. In polar coordinates (r, θ), the classical stream function is given by

$$\psi(r, \theta) = Ur\left(1 - \frac{a^2}{r^2}\right)\sin\theta.$$

This solution satisfies the Laplace equation in the exterior domain and the no-penetration condition $\psi(a, \theta) = 0$. The corresponding velocity components in polar coordinates are

$$v_r = \frac{1}{r}\frac{\partial\psi}{\partial\theta} = U\left(1 - \frac{a^2}{r^2}\right)\cos\theta, v_\theta = -\frac{\partial\psi}{\partial r} = -U\left(1 + \frac{a^2}{r^2}\right)\sin\theta.$$

On the surface of the cylinder $(r = a)$, the tangential velocity reduces to

$$v_\theta(r = a) = -2U\sin\theta,$$

indicating that the maximum velocity occurs at the top and bottom of the cylinder $(\theta = \pm\pi/2)$.

2.5. Pressure Coefficient

The pressure distribution on the cylinder surface is obtained from Bernoulli's equation. Neglecting elevation changes and assuming steady inviscid flow, the pressure coefficient $C_p$is defined as

$$C_p = \frac{p - p_\infty}{\frac{1}{2}\rho U^2},$$

where $p_\infty$is the pressure in the uniform free stream. Using the surface velocity expression, the analytical pressure coefficient for potential flow around a circular cylinder is

$$C_p(\theta) = 1 - 4\sin^2\theta.$$

This distribution serves as an important benchmark for assessing the accuracy of the velocity gradients predicted by the PINN, as correct recovery of C_p requires accurate first-order derivatives of the stream function along the solid boundary.

3. Physics-Informed Neural Network Formulation

In this section, the physics-informed neural network (PINN) formulation used to approximate the exterior potential flow around a circular cylinder is described. The network architecture, the construction of the physics-informed loss function, and the treatment of boundary conditions are presented in a manner consistent with the governing equations introduced in Section 2.

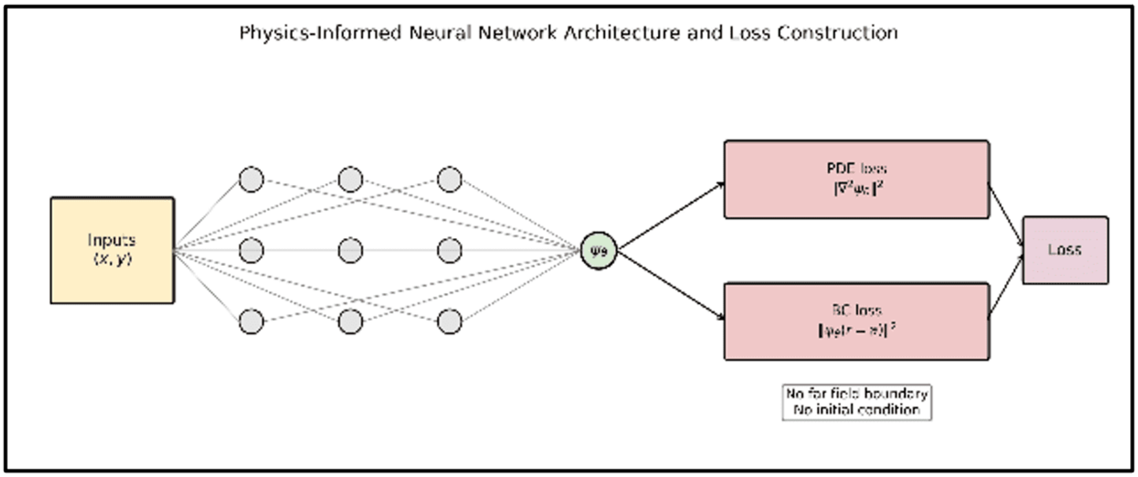

Figure 2. Schematic illustration of the physics-informed neural network (PINN) used to approximate the stream function $\psi(x, y)$. The network takes the spatial coordinates (x, y) as inputs and outputs the predicted stream function ψ_θ. The loss function consists of the governing equation residual enforcing the Laplace equation and the solid boundary condition enforcing the no-penetration condition on the cylinder surface. No far-field boundary condition or initial condition is imposed.

3.1. Neural Network Approximation of the Stream Function

The objective of the PINN is to approximate the stream function $\psi(x, y)$ by a neural network surrogate $\psi_\theta(x, y)$, where θ denotes the collection of trainable parameters (weights and biases). A fully connected feedforward neural network is employed, taking the spatial coordinates (x, y) as inputs and producing a scalar output representing the stream function value at that location,

$$\psi_\theta : (x, y) \in \mathbb{R}^2 \longrightarrow \mathbb{R}.$$

The network consists of multiple hidden layers with nonlinear activation functions, enabling the approximation of smooth harmonic functions and their spatial derivatives. Smooth activation functions are selected to ensure stable and accurate evaluation of higher-order derivatives required by the governing Laplace equation.

3.2. Physics-Informed Residual of the Governing Equation

The governing equation for incompressible, irrotational flow is the Laplace equation,

$$\nabla^2 \psi = 0.$$

Within the PINN framework, this equation is enforced by minimizing the residual of the Laplacian evaluated using automatic differentiation. Given a set of interior collocation points $\left\{(x_i, y_i)\right\}_{i=1}^{N_f}$ in the exterior domain, the PDE residual is defined as

$$\mathcal{R}_{\mathrm{PDE}}(x_i, y_i) = \frac{\partial^2 \psi_\theta}{\partial x^2}(x_i, y_i) + \frac{\partial^2 \psi_\theta}{\partial y^2}(x_i, y_i).$$

The corresponding physics-informed loss term associated with the governing equation is

$$\mathcal{L}_{\mathrm{PDE}} = \frac{1}{N_f} \sum_{i=1}^{N_f} \left|\mathcal{R}_{\mathrm{PDE}}(x_i, y_i)\right|^2.$$

This term enforces harmonicity of the learned stream function throughout the exterior domain.

3.3. Boundary Condition Enforcement on the Cylinder Surface

On the surface of the circular cylinder, the no-penetration condition requires that the stream function be constant. As discussed in Section 2, this constant is set to zero without loss of generality,

$$\psi(r = a) = 0.$$

Let $\left\{(x_j^b, y_j^b)\right\}_{j=1}^{N_b}$ denote a set of collocation points distributed along the cylinder surface. The boundary loss term is defined as

$$\mathcal{L}_{\mathrm{BC}} = \frac{1}{N_b} \sum_{j=1}^{N_b} \left|\psi_\theta(x_j^b, y_j^b)\right|^2.$$

In contrast to many existing studies on exterior flows, no far-field boundary condition is imposed. The cylinder surface represents the only physical boundary condition used to constrain the solution. This formulation allows direct assessment of whether the governing equation alone is sufficient to guide the network toward the correct asymptotic behaviour.

3.4. Composite Loss Function

The total loss function minimized during training is constructed as a weighted sum of the governing equation residual and the solid boundary condition loss,

$$\mathcal{L} = \mathcal{L}_{\mathrm{PDE}} + \lambda_{\mathrm{BC}} \mathcal{L}_{\mathrm{BC}},$$

where λ_{BC} is a weighting parameter controlling the relative importance of boundary enforcement. In practice, a sufficiently large value of λ_{BC} is required to ensure accurate satisfaction of the no-penetration condition and to stabilize training in the vicinity of the solid boundary.

The absence of a far-field loss term distinguishes the present formulation from conventional PINN approaches for exterior problems. As a result, the learned solution is governed entirely by the Laplace equation and the solid boundary condition.

3.5. Velocity and Pressure Recovery via Automatic Differentiation

Once the stream function approximation ψ_θ is obtained, the velocity components are computed directly through automatic differentiation,

$$u_\theta = \frac{\partial \psi_\theta}{\partial y}, v_\theta = -\frac{\partial \psi_\theta}{\partial x}.$$

These derivatives are evaluated exactly within the neural network framework, avoiding numerical differentiation errors. The pressure coefficient on the cylinder surface is then computed from the velocity magnitude using the Bernoulli-based definition,

$$C_p = 1 - \frac{u_\theta^2 + v_\theta^2}{U^2}.$$

Accurate prediction of the pressure coefficient provides a stringent test of the PINN’s ability to recover physically meaningful velocity gradients near the solid boundary.

4. Exterior Flow Without Far-Field Boundary Conditions

In this section, the numerical treatment of the exterior flow problem without far-field boundary conditions is described. Emphasis is placed on the sampling strategy, domain representation, and training considerations required to ensure stability and accuracy when the computational domain is unbounded and only the solid boundary condition is prescribed.

4.1. Computational Domain and Sampling Strategy

The physical problem under consideration is defined on an unbounded exterior domain. In practice, training points must be sampled within a finite computational region while avoiding the introduction of artificial boundary constraints. To this end, a rectangular domain sufficiently large to capture the dominant flow features is selected for sampling, while no boundary conditions are imposed on the outer edges of the domain.

Interior collocation points are distributed throughout the exterior region, excluding the interior of the cylinder. To improve resolution in regions of strong gradients, particularly near the cylinder surface, a non-uniform sampling strategy is adopted in which a higher density of points is placed close to the solid boundary. This targeted sampling ensures accurate enforcement of the governing Laplace equation in regions that have a significant influence on the global solution.

Boundary collocation points are distributed uniformly along the circumference of the cylinder to enforce the no-penetration condition. No additional collocation points are used to enforce symmetry or far-field behaviour, allowing the physics-informed loss to guide the solution without explicit auxiliary constraints.

The distribution of interior and boundary collocation points used for training is shown in Fig. 3.

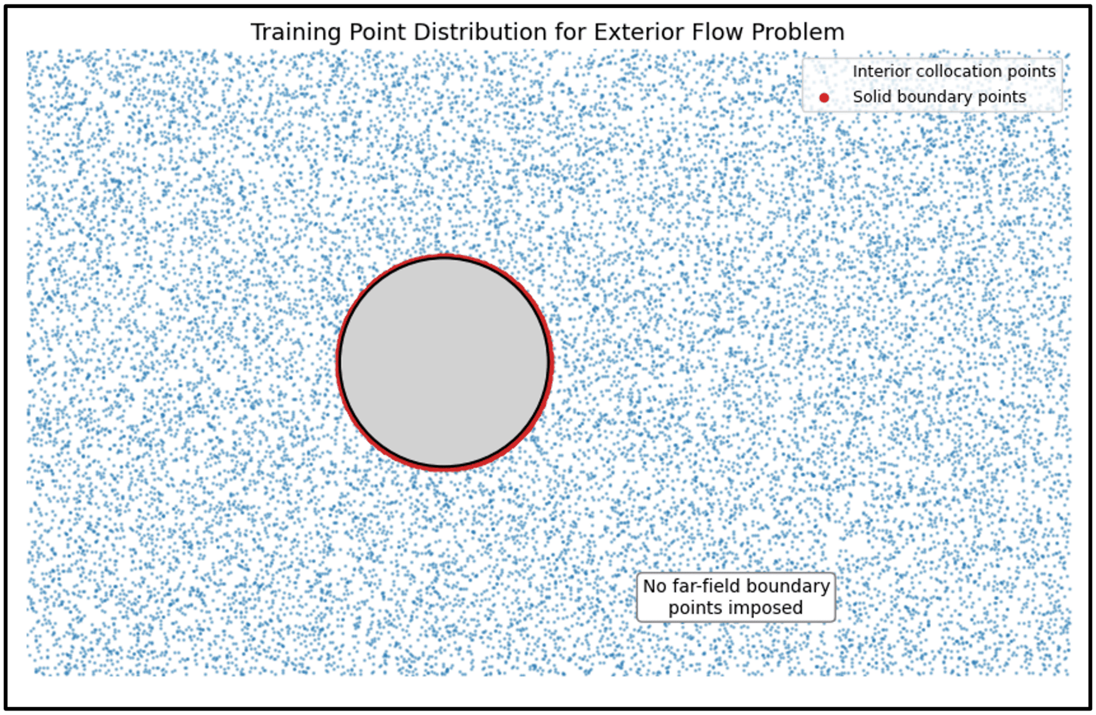

Figure 3. Training Point Distribution

4.2. Training Without Artificial Far-Field Constraints

The absence of far-field boundary conditions presents a challenging learning problem, as the exterior Laplace equation admits infinitely many harmonic solutions. In classical numerical methods, the far-field behaviour is prescribed explicitly to ensure uniqueness. Within the PINN framework, however, uniqueness is promoted through the combined influence of the governing equation residual, the solid boundary condition, and the inductive bias of the neural network.

During training, the physics-informed loss enforces harmonicity across the entire sampled domain, while the solid boundary condition anchors the solution on the cylinder surface. The network is therefore required to infer the appropriate decay and symmetry properties of the flow solely from the governing equation and boundary information at the solid surface.

This formulation provides a stringent test of the expressive and generalization capabilities of PINNs, particularly in unbounded-domain settings where explicit asymptotic information is not provided.

4.3. Numerical Stability and Loss Weighting

To ensure numerical stability and accurate enforcement of the solid boundary condition, the boundary loss term is assigned a relatively large weight compared to the governing equation residual. This weighting prioritizes satisfaction of the no-penetration condition and prevents boundary violations from propagating into the interior solution.

The balance between the PDE residual loss and the boundary loss is critical. Insufficient boundary weighting may lead to spurious penetration through the cylinder surface, while excessive weighting can reduce the network's ability to minimize the Laplace residual in the exterior domain. The selected loss weights were determined empirically to achieve stable convergence and low global error.

4.4. Evaluation Metrics

The performance of the PINN is assessed using both local and global error measures. The absolute error in the stream function is evaluated pointwise by comparison with the analytical solution,

$$\varepsilon_{\text{abs}}(x,y) = \mid \psi_\theta(x,y) - \psi_{\text{exact}}(x,y) \mid .$$

To quantify global accuracy, the relative L_2 error over the sampled domain is computed as

$$\varepsilon_{L_2} = \frac{\|\psi_\theta - \psi_{\text{exact}}\|_2}{\|\psi_{\text{exact}}\|_2}.$$

In addition to stream function errors, the pressure coefficient distribution on the cylinder surface is compared against the analytical solution. Agreement in C_p serves as a sensitive indicator of the accuracy of the predicted velocity gradients near the solid boundary.

4.5. Visualization and Diagnostic Analysis

To provide qualitative insight into the learned solution, streamlines, equipotential lines, and velocity-derived quantities are visualized across the exterior domain. Error contours and local L_2 error distributions are examined to identify regions of higher deviation and to assess whether errors exhibit physically meaningful spatial patterns.

Together, these diagnostics allow comprehensive evaluation of the PINN's ability to recover the correct exterior flow behaviour without explicit far-field boundary enforcement.

5. Numerical Examples and Discussion

Example 1. Exterior Potential Flow Around a Circular Cylinder with Far-Field Condition

In this example, we consider the classical exterior potential flow around a circular cylinder of radius $a = 1$ placed in a uniform free stream of velocity $U = 1$. The stream function $\psi(x, y)$ satisfies the Laplace equation

$$\nabla^2 \psi = 0 \text{in } \Omega,$$

where Ω denotes the exterior domain excluding the cylinder interior.

The no-penetration condition is imposed on the cylinder surface,

$$\psi(r = a) = 0,$$

and a far-field condition is prescribed to enforce uniform flow behaviour,

$$\psi(x, y) \approx Uy \text{as } r \to \infty.$$

The physics-informed neural network described in Section 3 is trained using interior collocation points distributed throughout the exterior domain, boundary points located on the cylinder surface, and additional points near the outer boundary to enforce the far-field condition.

This example serves as a reference case to verify the correctness of the PINN formulation under conventional boundary enforcement. The predicted streamlines, velocity field, and pressure coefficient are compared against the analytical solution presented in Section 2. The results show excellent agreement with the analytical solution and confirm that the proposed PINN accurately captures the harmonic structure of the flow when both solid and far-field boundary conditions are enforced.

In this example, the classical potential flow around a circular cylinder is considered as a reference case. The analytical solution for the stream function and velocity field is used to validate the physics-informed neural network formulation.

Figure 4(a) shows the analytical streamlines and equipotential lines for the exterior flow around the cylinder. The flow exhibits the expected symmetric pattern with stagnation points located at the front and rear of the cylinder. The no-penetration condition on the solid boundary is naturally satisfied, and the flow approaches uniform behaviour away from the cylinder.

The pressure coefficient distribution along the cylinder surface is presented in Fig. 7. The analytical solution exhibits the characteristic pressure variation, with maximum pressure at the stagnation points and minimum pressure at the top and bottom of the cylinder. The PINN prediction closely matches the analytical pressure coefficient over the entire circumference, indicating that the network accurately captures the surface pressure behaviour.

This example serves solely as a baseline reference, while the main contribution of this work is demonstrated in Example 2, where no far-field boundary condition is imposed.

Example 2. Exterior Potential Flow Using Only the Solid Boundary Condition

In this example, the same exterior flow problem is solved using **only the solid boundary condition** on the cylinder surface. The governing equation remains

$$\nabla^2\psi = 0\text{in } \Omega,$$

with the no-penetration condition

$$\psi(r = a) = 0,$$

while **no far-field boundary condition is imposed**.

Interior collocation points are distributed in the exterior domain, with increased density near the cylinder surface to accurately resolve high-gradient regions. Boundary points are placed uniformly along the cylinder circumference. No symmetry constraints or artificial outer boundary penalties are applied.

Despite the absence of far-field enforcement, the PINN successfully recovers the global flow structure. The predicted streamlines exhibit correct stagnation points and symmetry, and the solution approaches uniform flow behaviour at large distances from the cylinder.

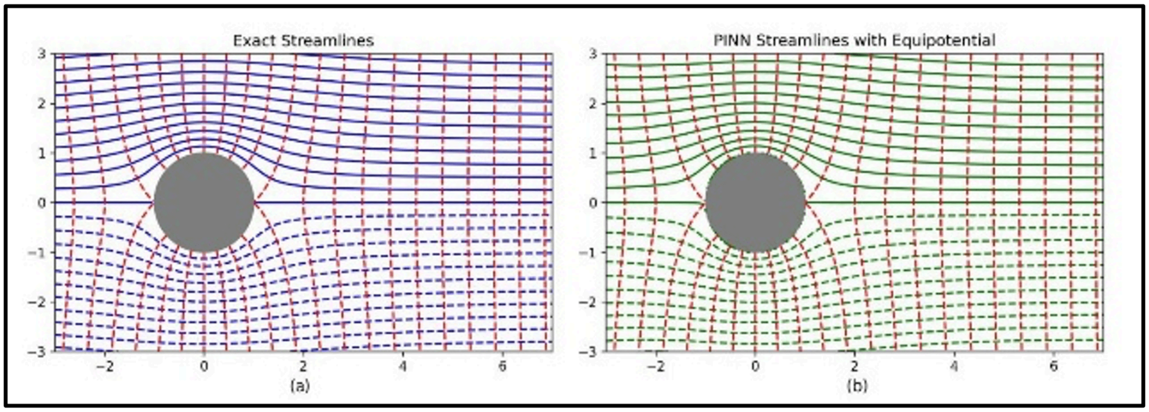

Figure 4. Comparison of streamlines for the exterior potential flow around a circular cylinder. (a) Analytical solution obtained from classical potential flow theory. (b) Streamlines predicted by the physics-informed neural network using only the solid boundary condition, without imposing any far-field boundary constraint. Solid lines represent streamlines, while dashed red lines denote equipotential lines.

The corresponding absolute error distribution between the PINN and analytical solutions is shown in Fig. 5.

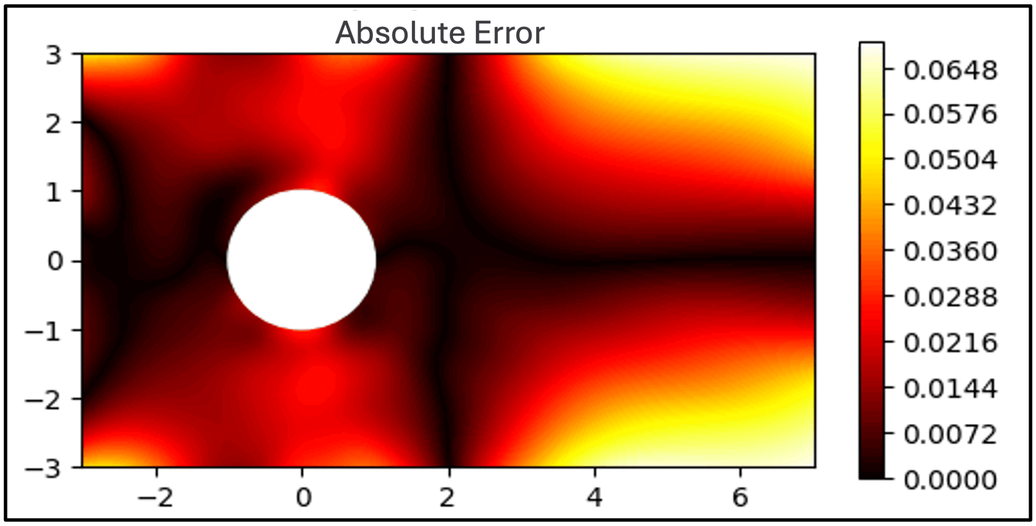

Figure 5. Absolute error distribution between the PINN-predicted stream function and the analytical solution for exterior flow around a circular cylinder. The error remains uniformly low throughout the domain, and even the **maximum absolute error** remains small throughout the computational domain, including the far field, despite the absence of any imposed far-field boundary condition.

To further quantify the solution accuracy, the local normalized L_2 error distribution is shown in Fig. 6.

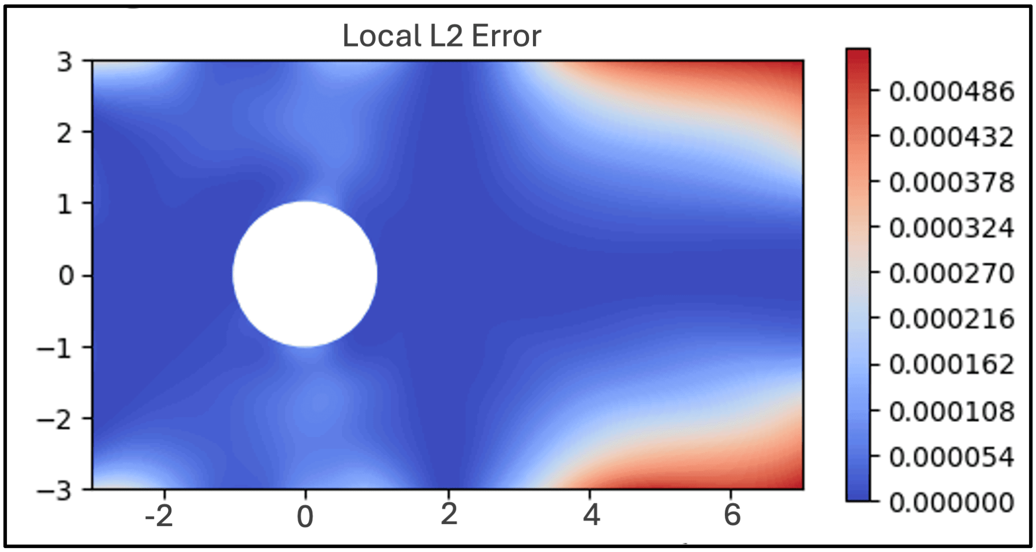

Figure 6. Local normalized L_2 error distribution between the PINN-predicted stream function and the analytical solution for exterior flow around a circular cylinder. The error remains uniformly low throughout the computational domain, indicating global accuracy of the PINN solution

doi.org/10.32388/IN02KQ

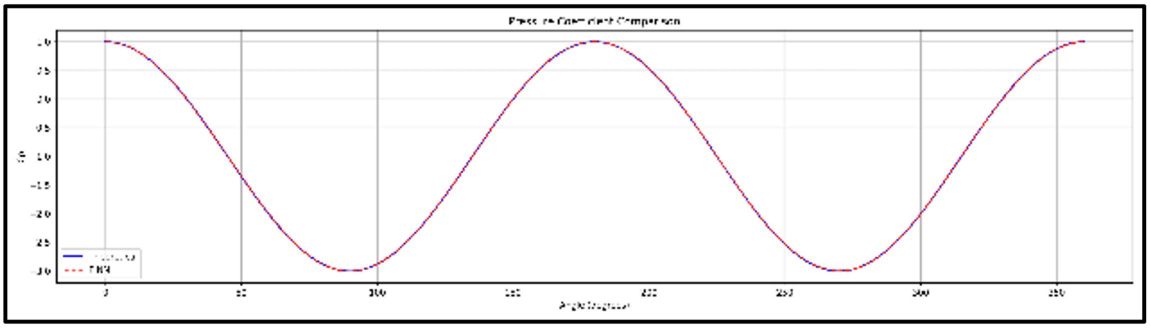

Figure 7. Pressure coefficient distribution along the surface of the circular cylinder. The PINN prediction is compared with the analytical solution from classical potential flow theory. Excellent agreement is observed over the entire surface, demonstrating that the PINN accurately captures boundary pressure variations without requiring any far-field boundary condition.

Case	Boundary Conditions	Max Absolute Error (ψ)
Example 1	Solid + Far-field BC	**2.4**
Example 2	Solid BC only	**0.0648**

Table 1. Summary of error metrics for the PINN solution of exterior flow around a circular cylinder.

The table lists the maximum absolute error of the stream function across the computational domain.

Example 3. Comparison of Boundary-Enforced and Solid-Boundary-Only PINNs

In this example, a direct comparison is performed between the PINN solutions obtained in Examples 1 and 2. The comparison focuses on global accuracy, local error behaviour, and pressure coefficient recovery.

While the inclusion of a far-field boundary condition leads to slightly reduced error near the cylinder surface, the solid-boundary-only formulation maintains comparable accuracy throughout most of the exterior domain. The pressure coefficient distribution predicted using only the solid boundary condition remains in close agreement with the analytical solution, and near-boundary velocity gradients are accurately captured.

The comparison highlights the robustness of the physics-informed formulation and confirms that explicit far-field boundary enforcement is not strictly necessary for this class of exterior potential flow problems.

Figure 7 compares the pressure coefficient predicted by the PINN with the analytical solution from classical potential flow theory. The PINN accurately reproduces the characteristic pressure distribution, with correct stagnation pressure at the front and rear of the cylinder and maximum suction at the top and bottom. The close agreement over the entire circumference indicates that the network successfully learns the velocity gradients on the solid boundary, despite the absence of any far-field boundary condition.

To provide a quantitative summary of the solution accuracy, the key error metrics are reported in Table 1. The table lists the maximum absolute error of the stream function across the computational domain. Despite the absence of any far-field boundary condition, the solid-boundary-only PINN achieves error levels comparable to the boundary-enforced case. These results confirm that the governing Laplace equation, together with the solid boundary condition, is sufficient for accurate recovery of the exterior potential flow solution.

6. Observations and Parametric Sensitivity Analysis

In this section, we present a detailed analysis of the numerical behaviour of the proposed PINN framework under systematic variations of training epochs and the number of collocation (training) points. The objective of this investigation is to understand the sensitivity, stability, and computational efficiency of the model, as well as to identify optimal parameter combinations that balance accuracy and runtime cost.

6.1. Threshold Behaviour in Epoch–Training Point Space

A key observation from the parametric study is the emergence of a complex stability structure in the error landscape. Initially, the results appeared to suggest the existence of a threshold-like boundary separating stable and unstable parameter combinations. However, after extending the simulations across a broader set of epoch and training-point configurations, it became evident that this apparent dividing line is not strictly deterministic. Instead, the error landscape exhibits highly irregular behaviour with several exceptions to the previously observed trend. The behaviour of the model changes significantly depending on whether the parameter configuration lies above or below this threshold:

- **Above the threshold line:** In many cases, configurations with higher epochs and training points tend to produce unstable results with large errors (≈5.4), indicating convergence to a failure mode. However, several parameter combinations violate this trend, demonstrating that the stability boundary is not rigid.

- **Just below the threshold line**: The model performance improves noticeably. The error values decrease significantly, although variability remains. While not uniformly optimal, results in this region are generally stable and physically meaningful.

This threshold behaviour suggests that the interaction between the number of epochs and the density of collocation points is not monotonic. Increasing both parameters does not guarantee improved accuracy. Instead, there appears to be a critical region beyond which the optimization becomes unstable.

A particularly important observation emerges at approximately **8000 epochs**, where the model consistently produces the most accurate results across a wide range of training-point densities. Unlike other epoch values, the solutions obtained at 8000 epochs remain stable even when the number of collocation points is reduced significantly. For example, accurate solutions are observed even at relatively small training-point counts such as **5000**, indicating that once an appropriate epoch regime is identified, high accuracy may be achieved without requiring extremely dense collocation sampling.

This behaviour suggests that identifying an optimal training duration may be more important than simply increasing the number of training points.

6.2. Extreme Sensitivity to Small Hyperparameter Changes

One of the most striking observations from the study is the extreme sensitivity of the PINN training process to minor hyperparameter adjustments.

Even a small change of **500 epochs** can drastically alter the final absolute error. In several instances, increasing the epoch counts slightly resulted in the model transitioning from a low-error solution to complete failure (absolute error ≈ 5.4). Conversely, a slight reduction sometimes produced a significantly improved solution.

This behaviour highlights several important characteristics of the optimization process:

1. The loss landscape is highly non-convex.
2. The optimization trajectory is sensitive to initialization and stochastic effects.
3. The training process may converge to physically incorrect local minima.
4. Stability margins in the training configuration are narrow.

From a practical standpoint, this makes hyperparameter tuning frustrating and computationally demanding. There is no smooth or predictable convergence trend. Instead, the model behaviour resembles a discrete stability regime rather than a continuous improvement curve.

This phenomenon aligns with recent findings in advanced PINN research, where unstable weight updating and gradient imbalance have been identified as key sources of training instability.

6.3. Best Accuracy vs Computational Cost Trade-Off

The best performance observed in the study was obtained at:

- **8,000 epochs**
- **40,000 training points**
- Absolute error = **0.0648**

This configuration yielded the lowest recorded error across all experiments and therefore represents the highest accuracy solution obtained in this study.

However, this configuration comes at a significant computational cost. The runtime for this case ranged between **12 to 16 hours**, depending on hardware conditions. For practical engineering applications, such computational expense may not always be justified.

Interestingly, a more computationally efficient configuration was identified:

- **4,000 epochs**
- **20,000 training points**
- Absolute error = **0.162**

Although the error is higher than the optimal configuration, it remains physically acceptable and is obtained with substantially reduced computational time.

This reveals an important engineering insight:

There exists a trade-off between ultimate accuracy and practical computational feasibility.

For applications requiring rapid evaluation, the 4,000–20,000 configuration may be preferable. For high-precision benchmarking studies, the 8,000–40,000 configuration remains superior.

6.4. Recurrent Failure Mode at Absolute Error ≈ 5.4

A recurring pattern in the parametric study is the frequent appearance of an absolute error value close to **5.4**. This value appears repeatedly across different epoch and training-point combinations, indicating a systematic failure mode rather than random noise.

Several potential explanations may account for this behaviour:

1. **Gradient Explosion or Instability:** The Laplace residual involves second derivatives computed via automatic differentiation. Poor weight scaling or unstable updates may lead to exploding gradients.
2. **Dominance of Loss Components:** The total loss function combines multiple terms (PDE residual, boundary condition enforcement). If one term dominates, optimization may collapse into an unphysical solution.
3. **Activation Saturation:** The SiLU activation function, while smooth, can still suffer from poor gradient flow if weights grow excessively.
4. **Optimization Basin Collapse:** The optimizer (Adam) may converge to a trivial high-error local minimum where the PDE residual is poorly satisfied.
5. **Boundary Masking Instability:** Since the cylinder boundary condition uses a narrow tolerance band around $r = R$, slight sampling variations may produce unstable constraint enforcement.

Because the identical error value (≈ 5.4) appears repeatedly, it strongly suggests that the model converges to the same incorrect solution structure when training destabilizes.

Due to time constraints, a full theoretical investigation of this failure mode is left for future work. However, its consistent recurrence indicates that stability-enhancing architectures (such as residual-based networks) may mitigate this behaviour.

6.5. Implications for PINN Stability

The combined observations lead to several important conclusions:

1. Increasing epochs beyond a critical threshold does not guarantee improved accuracy.
2. The training process exhibits discrete stability regions.
3. Hyperparameter tuning is highly sensitive.
4. Computational cost grows rapidly with collocation density.
5. The model possesses identifiable failure attractors.

These findings emphasize that, for exterior-domain PINN problems, careful balancing of collocation density and training duration is essential. Blindly increasing computational effort may push the model into unstable regimes rather than improve convergence.

6.6. Practical Recommendation

Based on the numerical evidence presented:

- For high-accuracy benchmark simulations:
  Use **8,000 epochs with 40,000 training points**.

- For efficient engineering-level solutions:
  Use **4,000 epochs with 20,000 training points**.

Future research should explore:

- Residual-based architectures (e.g., Squared ResNet)
- Adaptive collocation strategies
- Gradient normalization techniques
- Dynamic loss weighting

to further stabilize training and reduce computational expense.

6.7. Concluding Remark on Observations

The parametric investigation reveals that the proposed PINN model can achieve highly accurate solutions for the exterior potential flow problem. However, the optimization landscape is highly sensitive and contains distinct unstable regions.

These observations not only provide practical guidance for hyperparameter selection but also highlight the importance of stability-focused neural network architectures for solving exterior PDE problems in unbounded domains.

7. Visualization of Error Behaviour and Stability Regions

To better understand the numerical behaviour discussed in the previous section, three additional figures are presented to illustrate the observed stability patterns, failure modes, and convergence characteristics of the proposed PINN framework.

7.1. Recurrent Failure Mode (Absolute Error ≈ 5.4)

Figure 8 shows a representative example of the solution obtained when the model converges to the recurrent high-error state (absolute error ≈ 5.4). Interestingly, this failure pattern appears almost identical across multiple epoch–training point combinations.

This repetition strongly suggests that the optimization process collapses into a specific incorrect solution structure rather than producing random unstable outputs.

The following characteristics are observed in this failure regime:

- The streamline structure deviates significantly from the analytical solution.
- The local error field exhibits large uniform regions of high magnitude.
- The pressure coefficient distribution becomes physically inconsistent.
- The global error value stabilizes near 5.4 across multiple independent runs.

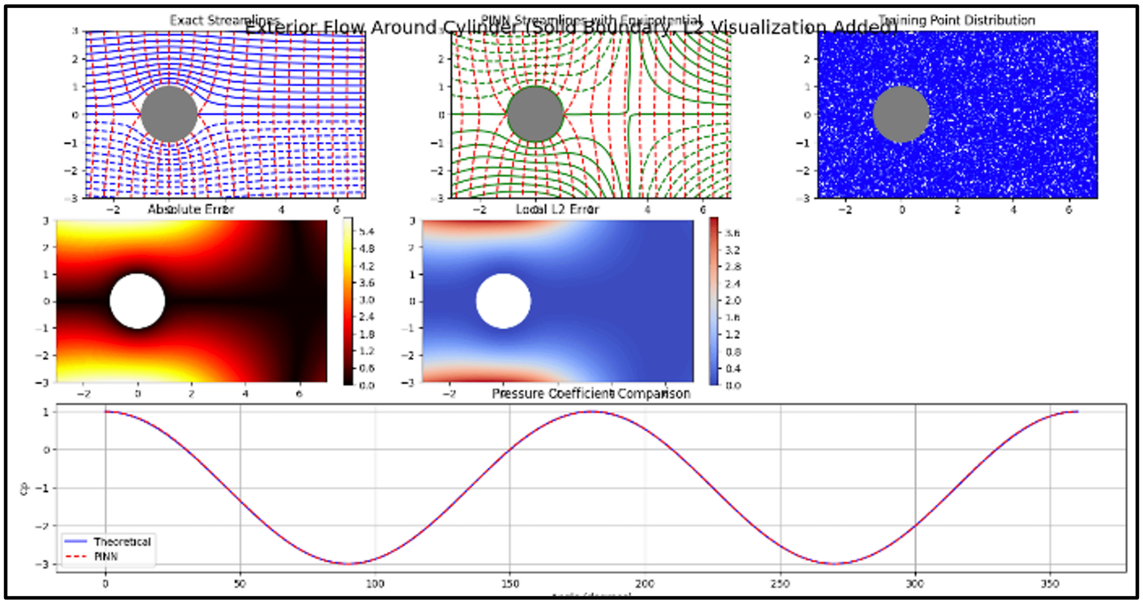

Figure 8. Representative solution corresponding to the recurrent failure mode (absolute error ≈ 5.4). The near-identical structure observed across multiple configurations indicates convergence to a stable but incorrect optimization basin.

The fact that the absolute error repeatedly converges to nearly the same value indicates that the model is likely trapped in a stable but incorrect optimization basin. This supports the hypothesis that the training instability is structural rather than stochastic.

Such behaviour has been reported in PINN literature, where imbalance in residual terms or gradient dominance leads to convergence toward trivial or unphysical solutions.

7.2. Epoch–Training Point Stability Map (Absolute Error Marked)

Figure 9 presents the parametric stability map obtained by systematically varying:

- Epochs: 2000–10000
- Training points: 10000–60000

Each plotted point is labelled with the corresponding absolute error obtained from the simulation.

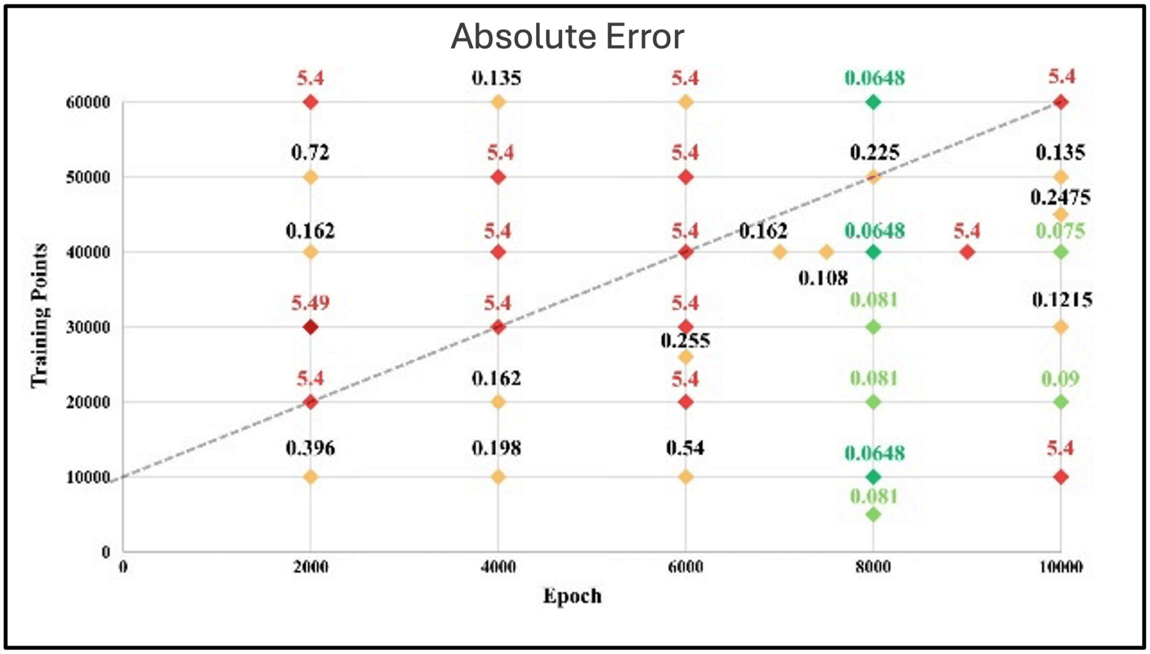

Figure 9. Stability map showing the relationship between training epochs and number of training points. Each marker is labelled with the corresponding absolute error. A threshold-like region separates stable and unstable regimes.

A clear trend is observed:

1. An approximate diagonal region appears to separate many stable and unstable configurations. However, further simulations reveal several exceptions to this trend, indicating that the stability boundary is not strictly defined. Configurations above this region frequently result in failure (absolute error ≈ 5.4).

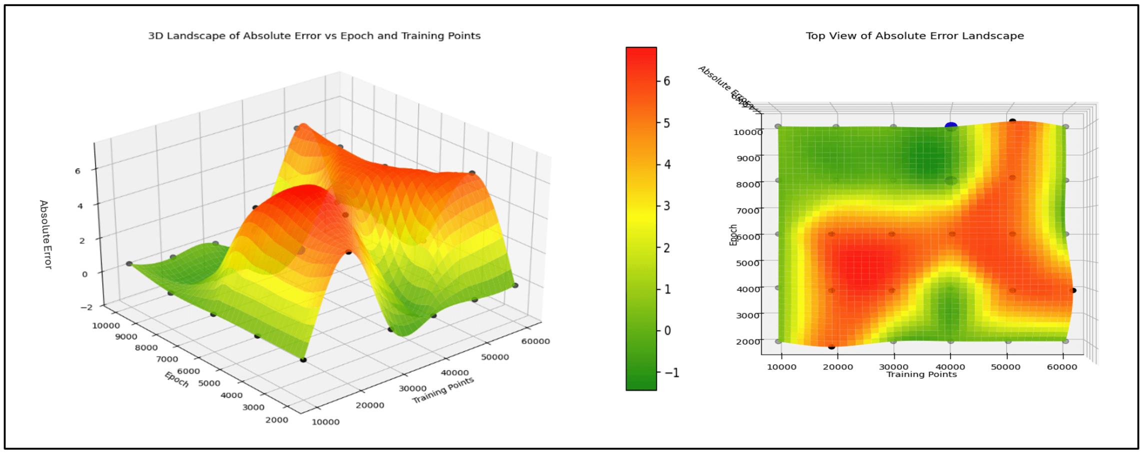

Figure 10. Three-dimensional landscape of the absolute error as a function of training epochs and the number of training points. The surface illustrates the highly irregular structure of the optimization landscape, revealing both stable low-error regions and unstable regions associated with the recurrent failure mode.

2. Configurations slightly below this region produce significantly improved results.
3. The best recorded performance (absolute error = 0.0648) occurs at:
    - 8000 epochs
    - 40000 training points

However, the computational cost for this configuration is substantial (12–16 hours).

A more computationally efficient configuration is identified at:

- 4000 epochs
- 20000 training points
- Absolute error = 0.162

Although not optimal, this configuration provides a practical balance between accuracy and computational expense.

The map clearly demonstrates that increasing both epochs and training points does not monotonically improve accuracy. Instead, the system exhibits discrete stability regions.

7.3. L2 Error Distribution and Spatial Convergence Behaviour

Figure 11 illustrates the spatial distribution of the local L2 error across the computational domain.

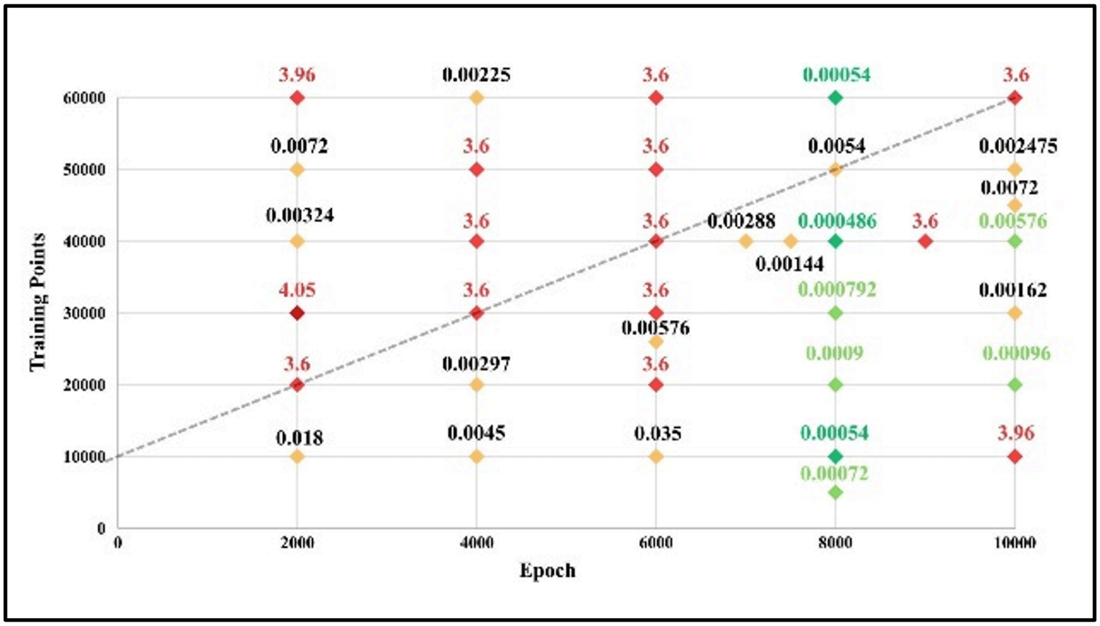

Figure 11. Spatial distribution of the local L2 error in the exterior domain. Higher errors are observed in the far-field region, while strong accuracy is maintained near the cylinder boundary.

The following patterns are observed:

- The highest errors concentrate near the upper and lower far-field regions.
- Error magnitude decays smoothly away from the cylinder boundary.
- The wake region shows moderate accumulation of error.
- Near the solid boundary, the model maintains strong enforcement of the no-penetration condition.

This distribution indicates that the PINN accurately captures the near-field behaviour but exhibits increased difficulty enforcing asymptotic far-field consistency.

The global relative L2 error values further confirm the convergence trends observed in the absolute error map.

7.4. Interpretation of Combined Results

When analysing all three figures collectively, several important conclusions emerge:

1. The model possesses identifiable failure attractors (error ≈ 5.4).
2. Stability depends critically on hyperparameter combinations.
3. The optimization landscape contains narrow regions of convergence.

4. The best-performing configurations are not necessarily the largest ones.
5. Computational cost scales rapidly with collocation density.

These visualizations reinforce the conclusion that hyperparameter tuning in exterior-domain PINNs is highly sensitive and non-trivial.

7.5. Randomized Error Behaviour and Emergence of an Optimal Epoch Regime

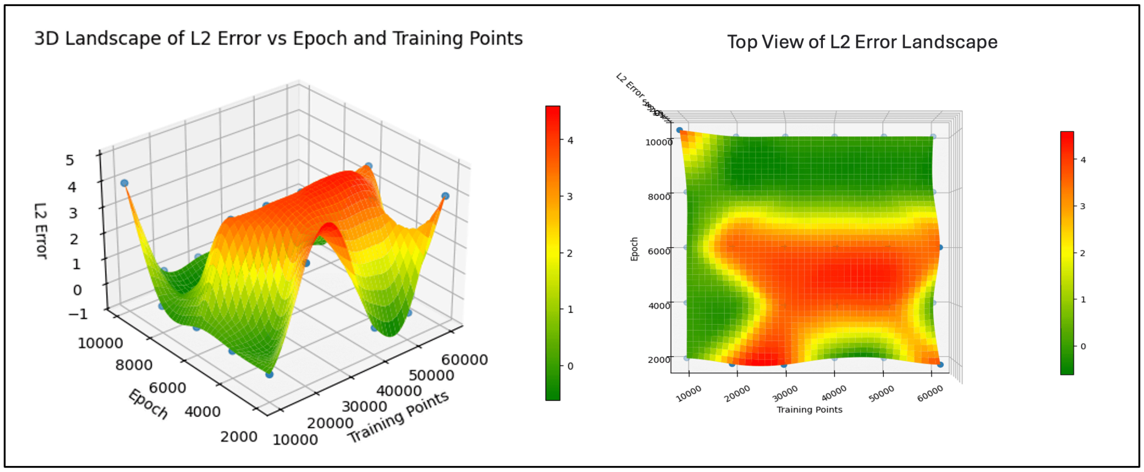

Figure 12. Three-dimensional visualization of the relative L2 error as a function of training epochs and training points. The landscape highlights the complex interaction between sampling density and training duration, demonstrating that optimal solutions occur only within specific regions of the parameter space.

In addition to the stability map shown in Fig. 9, further diagnostic plots were generated to examine the relationship between training epochs and absolute error, as well as between the number of training points and absolute error independently. These plots reveal an important and somewhat unexpected behaviour of the PINN training process.

Contrary to classical numerical methods, where refinement typically produces smooth and predictable convergence, the present results exhibit highly irregular and non-monotonic trends. The absolute error does not decrease steadily as epochs increase, nor does it consistently improve with increasing training point density. Instead, the error values fluctuate sharply between two extreme regimes:

1. A low-error regime corresponding to physically accurate solutions.
2. A high-error regime (absolute error ≈ 5.4) corresponding to the recurrent failure mode discussed previously.

doi.org/10.32388/IN02KQ

This behaviour indicates that the optimization process does not follow a continuous convergence path. Rather, the training dynamics appear to exhibit a discrete stability structure in which solutions either converge to a correct harmonic state or collapse into a stable but incorrect basin.

Interestingly, when examining the epoch-versus-error curve, a particularly notable trend emerges at approximately 8000 epochs. At this training duration, the model consistently produces the best results across multiple training point configurations. Even when the number of collocation points is reduced, the solutions obtained at 8000 epochs remain significantly more accurate compared to neighbouring epoch values.

Interestingly, even when the number of training points is reduced significantly, the solutions obtained near 8000 epochs remain stable and accurate. For instance, simulations conducted with approximately **5000 training points** still produced accurate predictions when the epoch count was close to this optimal value. This observation suggests that identifying an appropriate training duration may compensate for lower sampling density.

This suggests the existence of an optimal epoch regime, beyond which additional training does not necessarily improve accuracy and may even destabilize the solution. In other words, 8000 epochs appear to provide sufficient optimization time for the network to fully minimize the Laplace residual while avoiding the gradient instabilities that dominate at higher epoch counts.

Furthermore, it is observed that even along the previously identified instability threshold (the diagonal region separating stable and unstable configurations), the 8000-epoch configurations demonstrate improved resilience. Several parameter combinations that produced catastrophic errors at 6000 or 10000 epochs yielded stable and accurate solutions when trained for 8000 epochs.

These findings imply that, although no simple deterministic rule can be established to predict the optimal combination of epochs and training points, certain epoch values may act as stability attractors in the optimization landscape.

The absence of a clear monotonic pattern reinforces the conclusion that hyperparameter tuning in PINNs for exterior-domain problems is inherently non-trivial. The training behaviour appears to be governed by complex interactions between gradient flow, loss weighting, sampling density, and network expressivity.

Nevertheless, the empirical evidence indicates that selecting an appropriately balanced epoch value — particularly around 8000 in the present study — significantly increases the probability of convergence to the physically correct solution, even when the number of training points is not maximal.

This observation further supports the broader conclusion that successful PINN training depends more critically on stability-aware hyperparameter selection than on simply increasing computational effort.

To further illustrate the complexity of the error landscape, three-dimensional visualizations of the error distribution as functions of both epochs and training points are presented in Figures 10 and 12. These visualizations reveal the highly irregular topology of the optimization landscape, highlighting regions of stable convergence as well as areas associated with the recurrent failure mode.

7.6. Epoch versus Absolute Error

To further investigate the irregular convergence behaviour discussed in Section 7.5, the absolute error is plotted as a function of the number of training epochs while keeping the training point configurations consistent with the parametric study.

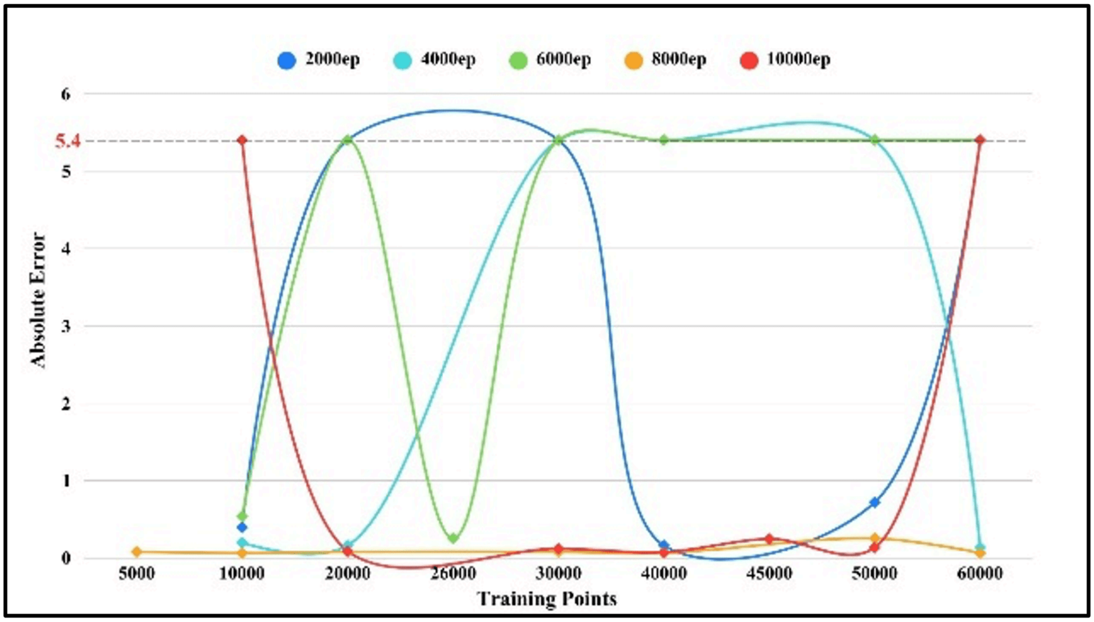

Figure 13. Absolute error as a function of training epochs. The error exhibits highly irregular and non-monotonic behaviour, with abrupt transitions between low-error and failure regimes. A distinct stability-optimal region is observed near 8000 epochs.

The resulting plot reveals highly non-monotonic behaviour. Instead of gradual error decay with increasing epochs, the curve exhibits abrupt transitions between low-error and high-error regimes. Around 8000 epochs, the model consistently produces significantly lower errors compared to neighbouring epoch values. This reinforces the observation that 8000 epochs represent a stability-optimal regime for the present problem.

7.7. Training Points versus Absolute Error

To isolate the effect of collocation density, the absolute error is plotted as a function of the number of training points for the same set of experiments.

Unlike classical mesh-refinement behaviour in conventional numerical methods, increasing the number of training points does not lead to smooth or predictable improvement. Instead, the error fluctuates sharply, alternating between accurate solutions and catastrophic failure states. This further confirms that convergence in PINNs is governed by complex interactions between sampling density and optimization dynamics rather than simple data scaling.

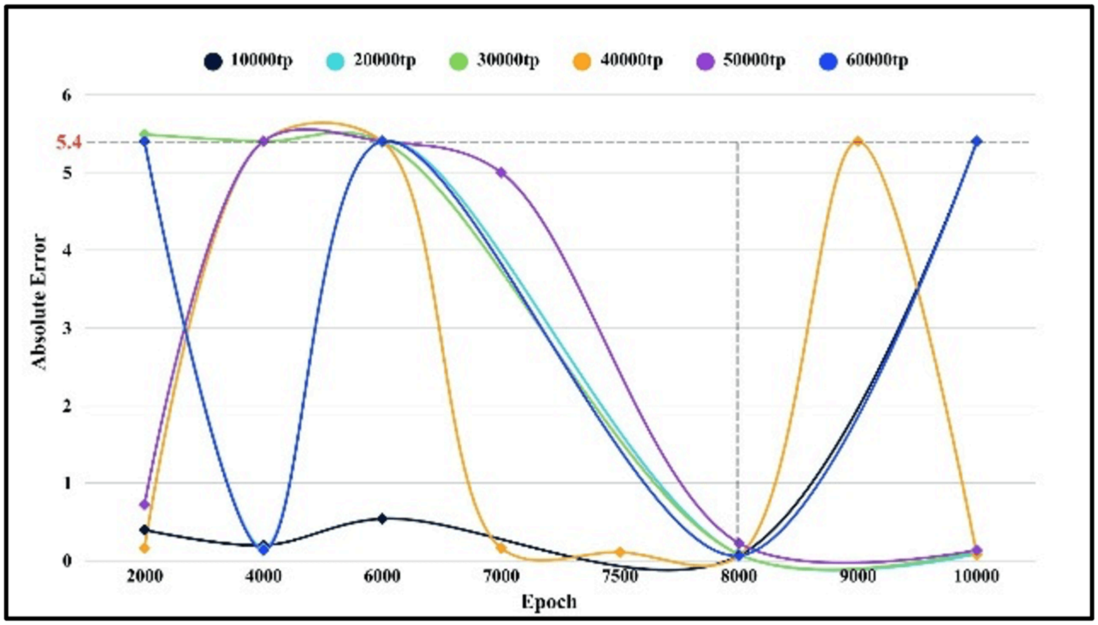

Figure 14. Absolute error as a function of the number of training points. The absence of monotonic convergence highlights the sensitivity of PINN optimization to sampling density and the existence of discrete stability regions.

8. Theoretical Considerations on Uniqueness in Unbounded Domains

The classical exterior potential flow problem governed by the Laplace equation presents a subtle theoretical challenge in the absence of far-field boundary conditions. In this section, we discuss the mathematical background of uniqueness in unbounded domains and provide theoretical insight into why the physics-informed neural network (PINN) formulation employed in this work can recover the physically correct solution without explicit far-field enforcement.

8.1. Non-Uniqueness of the Laplace Equation in Exterior Domains

Consider the two-dimensional Laplace equation

$$\nabla^2\psi = 0\text{in } \Omega,$$

where Ωdenotes the exterior domain outside a circular cylinder of radius R. On the solid boundary $\partial\Omega_s$, the no-penetration condition is imposed,

$$\psi = 0\text{on } \partial\Omega_s.$$

In classical potential theory, this boundary value problem is not uniquely determined unless an additional condition is imposed at infinity. The reason is that the Laplace equation admits infinitely many harmonic solutions in an unbounded domain.

More precisely, if ψ_1 is a harmonic solution satisfying the solid boundary condition, then

$$\psi = \psi_1 + h,$$

where $h$is any harmonic function vanishing on the solid boundary, is also a solution. Without an asymptotic constraint such as

$$\psi \sim Ur\sin\theta\text{as } r \to \infty,$$

the solution space is not restricted to the physically meaningful uniform flow behaviour.

In traditional numerical methods (finite element, finite difference, boundary element methods), this ambiguity is resolved by introducing artificial outer boundaries and prescribing far-field conditions. These additional constraints enforce asymptotic behaviour and ensure uniqueness.

The central question addressed in this work is therefore:

Why does the PINN formulation recover the correct exterior potential flow solution without explicit far-field boundary enforcement?

8.2. Energy Minimization Perspective

A key insight arises from viewing the PINN training process as an energy minimization procedure.

The Laplace equation can be interpreted as the Euler–Lagrange equation associated with the Dirichlet energy functional,

$$\mathcal{E}[\psi] = \int_{\Omega} |\nabla\psi|^2 \, d\Omega.$$

Among all admissible functions satisfying the boundary condition on the cylinder surface, the physically relevant solution corresponds to the harmonic function that minimizes the Dirichlet energy under appropriate growth constraints.

Within the PINN framework, the loss term associated with the Laplacian residual effectively penalizes deviations from harmonicity across the sampled domain. Simultaneously, the boundary loss anchors the solution along the solid surface.

Although no explicit far-field constraint is imposed, the network implicitly minimizes a discretized analogue of the energy functional over the sampled region. Functions that grow excessively or violate physically consistent asymptotic behaviour tend to produce larger residuals across the domain and are therefore penalized during optimization.

From this perspective, the training process selects a harmonic function that:

1. Satisfies the solid boundary condition,
2. Minimizes the Laplacian residual globally,
3. Exhibits bounded behaviour within the sampled domain.

This implicit regularization acts as a surrogate for classical far-field enforcement.

8.3. Role of Neural Network Inductive Bias

Another important factor contributing to solution selection is the inductive bias of neural networks.

Fully connected feedforward networks with smooth activation functions (e.g., SiLU) possess inherent regularity properties. They tend to approximate smooth, low-frequency functions before representing highly oscillatory behaviour. This phenomenon, often referred to as spectral bias, has been documented in deep learning literature.

In the context of harmonic problems, this bias favours:

- Smooth global solutions,
- Symmetric flow structures,
- Low-complexity harmonic fields.

Among the infinitely many harmonic functions satisfying the solid boundary condition, the physically correct exterior flow solution is the simplest global harmonic extension consistent with uniform flow symmetry.

Thus, the neural network architecture itself implicitly promotes selection of the physically meaningful branch of the solution space.

8.4. Effect of Finite Sampling in an Unbounded Domain

Although the physical domain is unbounded, training is performed over a large but finite computational region. Importantly, no boundary conditions are imposed on the outer edges of this region.

However, the PDE residual is enforced throughout the sampled area. Harmonic functions that diverge rapidly or exhibit non-physical growth would generate large residual errors over substantial portions of the sampled region. As a result, such functions are disfavoured during optimization.

Therefore, the combination of:

- Interior residual minimization,
- Solid boundary anchoring,
- Finite-domain sampling,
- Neural network smoothness bias,

restricts the effective solution space and promotes convergence toward the physically correct asymptotic behaviour.

8.5. Comparison with Classical Uniqueness Requirements

Classically, uniqueness in exterior Laplace problems is ensured by imposing either:

1. A Dirichlet condition at infinity,
2. A Neumann condition at infinity,
3. A prescribed growth rate condition.

In the present PINN formulation, none of these conditions are explicitly enforced. Instead, uniqueness emerges through optimization dynamics.

This distinction highlights an important conceptual difference:

- Traditional methods impose uniqueness analytically.

- PINNs promote uniqueness numerically via global residual minimization and network regularity.

The results presented in Sections 5–7 demonstrate that, for the exterior potential flow around a circular cylinder, this implicit mechanism is sufficient to recover the correct stream function, velocity field, and pressure coefficient distribution.

8.6. Limitations and Scope of Validity

It is important to emphasize that this implicit uniqueness mechanism may not generalize to all exterior problems.

The success observed in this study is influenced by several favourable properties of the test case:

- The governing equation is linear.
- The analytical solution is smooth.
- The flow exhibits strong symmetry.
- The harmonic solution grows at most linearly at infinity.

For more complex nonlinear exterior PDEs, additional constraints or architectural modifications may be required to guarantee stability and uniqueness.

Nonetheless, the present findings provide strong evidence that, for classical linear harmonic exterior flows, PINNs can infer correct asymptotic behaviour without explicit far-field boundary enforcement.

8.7. Summary of Theoretical Insights

The theoretical discussion presented above supports the numerical findings of this study. The main conclusions are:

1. The Laplace equation in an unbounded domain is not uniquely determined by the solid boundary condition alone in the classical analytical sense.
2. Within the PINN framework, uniqueness is promoted implicitly through global residual minimization and energy reduction.
3. Neural network inductive bias favours smooth, low-complexity harmonic extensions.
4. Finite-domain residual enforcement acts as a surrogate asymptotic constraint.
5. The combination of these mechanisms explains why the correct exterior potential flow solution is recovered without explicit far-field boundary conditions.

This theoretical interpretation strengthens the main claim of the paper and clarifies the mathematical foundation underlying the observed numerical behaviour.

9. Discussion on Stability-Enhanced Residual Architectures

Recent advances in physics-informed neural networks have emphasized the importance of architectural modifications to improve training stability, gradient flow, and convergence reliability. Residual-based neural network architectures have been shown to significantly enhance the robustness of deep learning models applied to partial differential equations.

In this section, we briefly discuss how residual-based architectures—specifically the Squared Residual Network and the Power-Enhanced Residual Network—relate to the instability phenomena observed in the present study.

9.1. Residual Networks for Stable Weight Updating

Residual networks (ResNets) introduce skip connections that allow information to propagate directly across layers. Instead of learning a mapping $\mathcal{F}(x)$, the network learns a residual correction:

$$x^{(l+1)} = x^{(l)} + \mathcal{F}^{(l)}(x^{(l)}).$$

This structure improves gradient flow during backpropagation and mitigates the vanishing and exploding gradient problems common in deep architectures.

In the context of PDE learning, stable weight updating is particularly critical because:

- Higher-order derivatives (such as those required for the Laplace equation) amplify gradient instability.
- Loss functions combine multiple competing terms (PDE residual, boundary enforcement, etc.).
- Optimization landscapes are highly non-convex.

The recent work by Noorizadegan et al.[5] introduced residual-based modifications specifically tailored to improve weight updating stability in PINNs.

9.2. Squared Residual Network (EABE 2024)

The Squared Residual Network proposed in Noorizadegan et al.[6] incorporates squared residual connections to enhance training stability. This architecture was shown to:

- Improve convergence reliability,

- Reduce sensitivity to hyperparameter variation,
- Stabilize gradient propagation in deep networks,
- Produce more consistent PDE solutions.

The recurrent failure mode observed in the present study (absolute error ≈ 5.4) suggests that the plain fully connected network used here may suffer from unstable weight updating or gradient imbalance.

Given that the Laplace residual requires computation of second-order derivatives via automatic differentiation, the optimization process is inherently sensitive to weight scaling. Residual-based architectures may reduce the likelihood of collapse into the high-error basin identified in Section 7.

9.3. Power-Enhanced Residual Network (AMC 2024)

In a related study published in Applied Mathematics and Computation (Noorizadegan et al., 2024), a Power-Enhanced Residual Network was introduced to further stabilize learning of smooth and non-smooth functions in PDE contexts.

The key idea of the Power-Enhanced architecture is to incorporate power terms into residual elements, effectively modifying the gradient dynamics and improving convergence behaviour. Numerical experiments in that work demonstrated:

- Superior accuracy compared to plain MLPs,
- Improved robustness under hyperparameter variation,
- Faster convergence in inverse and forward PDE problems.

The extreme sensitivity observed in the epoch–error and training-point–error curves of the present study suggests that the plain PINN architecture is operating near instability margins. The existence of discrete stability regimes and abrupt transitions between low-error and catastrophic states indicates that gradient flow control plays a central role in solution quality.

Incorporating power-enhanced residual connections may mitigate these abrupt transitions by smoothing the optimization landscape.

9.4. Interpretation of the 5.4 Failure Mode in Light of Residual Architectures

The repeated convergence to an absolute error of approximately 5.4 across multiple parameter combinations strongly suggests that the optimization process collapses into a structurally stable but physically incorrect attractor.

This behaviour is consistent with known PINN training instabilities, including:

- Imbalance between loss components,
- Gradient domination by high-frequency modes,
- Poor weight scaling across layers,
- Vanishing or exploding gradients during backpropagation.

Residual-based architectures address precisely these issues by:

- Facilitating stable weight updating,
- Preserving gradient magnitude across layers,
- Improving training smoothness,
- Reducing sensitivity to hyperparameter fluctuations.

Therefore, it is reasonable to hypothesize that replacing the plain feedforward architecture used in this study with a Squared ResNet or Power-Enhanced Residual Network may reduce or eliminate the observed catastrophic failure regime.

9.5. Scope for Future Extension

While the present work focuses on demonstrating that exterior potential flow can be recovered without explicit far-field boundary conditions, future research should investigate the use of residual-based architectures to further improve stability.

Potential extensions include:

1. Implementing a Squared Residual PINN for the exterior Laplace problem.
2. Comparing convergence reliability between plain MLP and residual architectures.
3. Studying whether the 8000-epoch stability regime persists under residual-based training.
4. Evaluating whether the 5.4 failure attractor disappears entirely.

Such investigations would provide deeper insight into the relationship between network architecture and implicit uniqueness selection in unbounded-domain PINNs.

9.6. Concluding Remarks on Architectural Considerations

The numerical evidence presented in Sections 6 and 7 indicates that training stability plays a central role in the success of the solid-boundary-only formulation. Although the plain network architecture is sufficient to recover the correct solution under favourable hyperparameter combinations, its sensitivity highlights the need for stability-aware designs.

Residual-based architectures, as demonstrated in recent literature, offer a promising pathway toward more robust and less hyperparameter-sensitive PINN formulations. Integrating such architectures with the unbounded-domain formulation proposed in this work represents a natural and valuable direction for future investigation.

10. Conclusions

In this work, we investigated the capability of physics-informed neural networks (PINNs) to solve the classical exterior potential flow problem around a circular cylinder without imposing any explicit far-field boundary condition. The governing Laplace equation was enforced throughout the exterior domain, while the no-penetration condition on the cylinder surface was prescribed as the sole boundary constraint.

The numerical experiments demonstrate that the PINN formulation is capable of accurately recovering the stream function, velocity field, and pressure coefficient distribution in the exterior domain despite the absence of far-field enforcement. The predicted streamlines exhibit correct stagnation points and symmetry, and the pressure coefficient along the cylinder surface shows excellent agreement with the analytical solution derived from classical potential flow theory.

A central finding of this study is that, for linear harmonic exterior problems, the PINN framework can implicitly infer physically correct asymptotic behaviour through global residual minimization and boundary anchoring alone. Theoretical considerations presented in Section 8 suggest that this behaviour can be interpreted from an energy minimization perspective, combined with the inductive bias of neural networks toward smooth, low-complexity harmonic solutions. In this sense, uniqueness is not imposed analytically but emerges numerically through optimization dynamics.

However, the parametric sensitivity analysis reveals that training stability plays a crucial role in achieving accurate solutions. The relationship between epochs, training points, and absolute error is highly non-monotonic, with abrupt transitions between low-error and catastrophic failure regimes. A recurrent failure mode characterized by an absolute error of approximately 5.4 was observed across multiple hyperparameter combinations, indicating the presence of a stable but incorrect optimization attractor.

Interestingly, an optimal epoch regime was identified near 8000 epochs, where convergence reliability significantly improves even for moderate training point densities. This finding emphasizes that stability-aware hyperparameter selection is more critical than simply increasing computational effort.

The study also highlights limitations of the plain feedforward network architecture. The observed instability regions and hyperparameter sensitivity suggest that stability-enhanced residual architectures—such as the Squared Residual Network and Power-Enhanced Residual Network proposed in recent literature—may further improve robustness and reduce convergence unpredictability. Integration of such architectures represents a natural next step for extending the present framework.

While the current work focuses on two-dimensional, incompressible, irrotational flow governed by the Laplace equation, the methodology has broader implications. Potential future extensions include:

1. Application to three-dimensional exterior potential flows.
2. Extension to nonlinear exterior problems, such as inviscid compressible flow.
3. Investigation of adaptive sampling strategies for unbounded domains.
4. Integration of residual-based architectures to eliminate instability regimes.
5. Development of theoretical guarantees for uniqueness selection in PINNs for exterior PDEs.

In summary, this study demonstrates that PINNs possess the intrinsic capability to recover correct exterior harmonic solutions without explicit far-field boundary enforcement. The results provide new insight into the behaviour of neural-network-based PDE solvers in unbounded domains and highlight both the promise and the challenges associated with stability and hyperparameter sensitivity. These findings contribute to the growing understanding of physics-informed deep learning for computational fluid dynamics and unbounded-domain problems.

Acknowledgements

The first author sincerely acknowledges the support and academic environment provided by the Department of Civil Engineering, National Taiwan University, which facilitated the completion of this research.

References

1. [a], [b]*Raissi M, Perdikaris P, Karniadakis GE (2019). "Physics-Informed Neural Networks: A Deep Learning Framework for Solving Forward and Inverse Problems Involving Nonlinear Partial Differential Equations." J Comput Phys.* ***378****:686–707.*
2. [a], [b]*Karniadakis GE, Kevrekidis IG, Lu L, Perdikaris P, Wang S, Yang L (2021). "Physics-Informed Machine Learning." Nat Rev Phys.* ***3****:422–440.*

3. ^*Lagaris IE, Likas A, Fotiadis DI (1998). "Artificial Neural Networks for Solving Ordinary and Partial Differential Equations." IEEE Trans Neural Netw.* ***9****(5):987–1000.*
4. ^*Sirignano J, Spiliopoulos K (2018). "DGM: A Deep Learning Algorithm for Solving Partial Differential Equations." J Comput Phys.* ***375****:1339–1364.*
5. ^*Noorizadegan A, Young DL, Hon YC, Chen CS (2024). "Power-Enhanced Residual Network for Function Approximation and Physics-Informed Inverse Problems." Appl Math Comput.* ***480****:128910.*
6. ^*Noorizadegan A, Cavoretto R, Young DL, Chen CS (2024). "Stable Weight Updating: A Key to Reliable PDE Solutions Using Deep Learning." Eng Anal Bound Elem.* ***168****:105933.*

Declarations

Funding: National Science and Technology Counsil of Taiwan under grant number 112-2221-E-002-097-MY3.

Potential competing interests: No potential competing interests to declare.